

# ESTIMATING CLIMATE CHANGE IMPACTS FROM ATMOSPHERIC CIRCULATION PATTERNS AND AIR MASSES

*A Paper From:*

**California Climate Change Center**

*Prepared By:*

**Scott Sheridan, Kent State University  
Katharine Hayhoe, Texas Tech University  
Laurence Kalkstein, University of Miami**

## DISCLAIMER

This paper was prepared as the result of work sponsored by the California Air Resources Board (ARB) and the California Environmental Protection Agency (Cal/EPA). It does not necessarily represent the views of the California Energy Commission, ARB, Cal/EPA, their employees, or the State of California. The Energy Commission, ARB, Cal/EPA, the State of California, their employees, contractors, and subcontractors make no warrant, express or implied, and assume no legal liability for the information in this paper; nor does any party represent that the uses of this information will not infringe upon privately owned rights. This paper has not been approved or disapproved by the California Energy Commission, ARB, or Cal/EPA, nor has the California Energy Commission, ARB, or Cal/EPA passed upon the accuracy or adequacy of the information in this paper.



California Environmental Protection Agency

**Air Resources Board**

*Arnold Schwarzenegger, Governor*

**DRAFT PAPER**

March 2009

CEC-500-2009-031-D



## **Acknowledgments**

We would like to acknowledge the California Air Resources Board for their financial support of this research.



## Preface

The California Energy Commission's Public Interest Energy Research (PIER) Program supports public interest energy research and development that will help improve the quality of life in California by bringing environmentally safe, affordable, and reliable energy services and products to the marketplace.

The PIER Program conducts public interest research, development, and demonstration (RD&D) projects to benefit California's electricity and natural gas ratepayers. The PIER Program strives to conduct the most promising public interest energy research by partnering with RD&D entities, including individuals, businesses, utilities, and public or private research institutions.

PIER funding efforts focus on the following RD&D program areas:

- Buildings End-Use Energy Efficiency
- Energy-Related Environmental Research
- Energy Systems Integration
- Environmentally Preferred Advanced Generation
- Industrial/ Agricultural/ Water End-Use Energy Efficiency
- Renewable Energy Technologies
- Transportation

In 2003, the California Energy Commission's PIER Program established the **California Climate Change Center** to document climate change research relevant to the states. This center is a virtual organization with core research activities at Scripps Institution of Oceanography and the University of California, Berkeley, complemented by efforts at other research institutions. Priority research areas defined in PIER's five-year Climate Change Research Plan are: monitoring, analysis, and modeling of climate; analysis of options to reduce greenhouse gas emissions; assessment of physical impacts and of adaptation strategies; and analysis of the economic consequences of both climate change impacts and the efforts designed to reduce emissions.

**The California Climate Change Center Report Series** details ongoing center-sponsored research. As interim project results, the information contained in these reports may change; authors should be contacted for the most recent project results. By providing ready access to this timely research, the center seeks to inform the public and expand dissemination of climate change information, thereby leveraging collaborative efforts and increasing the benefits of this research to California's citizens, environment, and economy.

For more information on the PIER Program, please visit the Energy Commission's website [www.energy.ca.gov/pier/](http://www.energy.ca.gov/pier/) or contract the Energy Commission at (916) 654-5164.



# Table of Contents

Preface..	iii
Abstract .....	viii
1.0 Description of Research .....	1
2.0 Background .....	2
3.0 Data and Methods .....	2
3.1. Upper-Air Circulation Fields .....	3
3.2. Principal Components and Cluster Analysis of Reanalysis and Climate Model Output .....	4
3.3. Spatial Synoptic Classification .....	5
3.4. Mortality Data .....	6
4.0 Results .....	7
4.1. Comparison of Reanalysis-based vs. AOGCM-based Circulation Patterns .....	7
4.2. Mortality Variability by Air Mass Across California .....	13
4.3. Historical Frequency of Oppressive Air Mass Occurrence by Reanalysis Cluster	13
5.0 Discussion and Conclusions .....	15
6.0 References .....	18
7.0 Glossary .....	20

## List of Figures

Figure 1. This map of the air masses covering the western part of the United States on June 21, 2008, shows most of California covered in a hot, “Dry Tropical” air mass that can likely be associated with increased wildfire risk, heat stress, and demand for air conditioning.....	3
Figure 2. Monthly frequency of ERA-40 and CCSM-based daily circulation patterns for 1958–2002. The proportion of days in each month belonging to each pattern is shown on the y-axis, while months are shown on the x-axis, from January (1) to December (12).....	10
Figure 3. Spatial patterns for matching ERA-40 and CCSM clusters based on 700 mb geopotential heights. Patterns are grouped by Summer (S), Summer Transitional (ST), Winter (W), and Winter Transitional (WT), while the number simply indicates the cluster number.....	12
Figure 4. Observed frequency of oppressive air mass days during the months of April to October by ERA-40 cluster for (a) inland cities, and (b) coastal cities.....	14

## List of Tables

Table 1. Spatial synoptic classification (SSC) classes and typical characteristics and geneses in California .....	6
Table 2. Population (year 2000) by age group for the California metropolitan areas studied in this research.....	7
Table 3. ERA-40 patterns and CCSM3-based matches .....	9
Table 3. Mean anomalous mortality (expressed as a percentage relative to the seasonal average) on Dry Tropical and Moist Tropical Plus days for the period of April–October for nine urban centers in California, separated by age (under 65, between 65 and 74, and over 74 years of age). Also shown are the average frequencies for which each air mass type (Dry Tropical and Moist Tropical Plus) occurs over each city during this period. A frequency of 10%, for example, means that 10% of the days from April to October fall into that air mass category. ....	13
Table 4. Proportion of oppressive air mass occurrence, by city and 700-mb cluster, for the ERA-40 reanalysis period of record from 1958–2002 for the warm season (April–October) .....	16



## Abstract

Anomalously hot and humid weather is often directly related to human-health and safety issues such as heat-related mortality, wildfires, and increased electricity demands. Typically, estimates of climate change impacts depend on projected changes in surface conditions. Here we explore the possibility that surface-level air masses associated with these impacts may be directly linked to upper-air circulation patterns. If so, we hypothesize that risks associated with certain impacts could be estimated without high-resolution surface climate projections.

We first identify dominant daily circulation patterns over North America using ERA-40 reanalysis of 500 millibar (mb), 700 mb, and 850 mb height and temperature fields. Twelve weather patterns are identified using an objective cluster analysis; two associated with oppressive air-mass events for coastal cities (typical of winter and transitional months) and three associated with oppressive air-mass events for inland cities (typical of summer conditions).

We compare these patterns with historical circulation patterns simulated by the National Center for Atmospheric Research's Community Climate System Model, version 3 (CCSM3), finding that the model is able to simulate recognizable spatial patterns and seasonal frequencies of the same dominant circulation patterns. This supports our hypothesis that global models are appropriate for use in prediction of large-scale circulation features, and it provides the basis for generating projected changes in oppressive air-mass events and impacts on heat-related mortality in California urban areas.

**Keywords:** Climate change, air mass, atmospheric circulation, heat stress, mortality, vulnerability



## 1.0 Description of Research

Surface weather conditions such as extreme temperature and humidity are directly related to the frequency and persistence of oppressive air masses. Human health and safety issues such as higher death rates due to the heat, the risk of wildfires, and increased demands for air conditioning can be linked to the frequency and persistence of these air masses.

Typically, estimates of climate change impacts depend on projections of changes in surface conditions. We hypothesize, however, that surface-level air masses known to be associated with specific impacts may be directly linked to upper-air circulation patterns. Furthermore, by predicting changes in these patterns, we may be able to obtain estimates of the probability of impacts under future climate change scenarios without the need to generate high-resolution surface climate projections.

This paper provides an initial exploration of this hypothesis through first identifying the dominant daily circulation patterns over North America using an objective cluster analysis on ERA-40 reanalysis of 500 millibar (mb), 700 mb, and 850 mb geopotential height and temperature fields. Next, we evaluate the extent to which these upper-air patterns can be correlated with surface-level oppressive air mass events associated with elevated levels of heat-related mortality in major California urban centers.

Interestingly, we find that the three circulation patterns associated with oppressive air mass events for coastal cities are typical of winter and transitional months. In contrast, the two circulation patterns associated with oppressive air mass events for inland cities are typical of summer conditions. This discovery suggests a possible difference in how climate change may affect coastal versus inland California cities, an observation with potentially important implications for future impacts.

Next, we assess whether a climate model has the capability to reproduce the observed spatial patterns and temporal frequencies of circulation patterns associated with oppressive air mass events. Using the same clustering technique to identify the dominant daily circulation patterns in NCAR CCSM3<sup>1</sup> historical 20C3M simulations, we find that CCSM3 is able to simulate recognizable spatial patterns and seasonal frequencies of the same dominant daily circulation patterns as identified in the reanalysis fields.

Building on these initial findings, our next steps are to develop quantitative projections of changes in frequency and intensity of these circulation patterns expected over the coming century, as simulated by multiple climate models under a range of future climate scenarios. We will then estimate climate change impacts on human health based on changes in circulation patterns and air mass frequency and intensity, and compare these with previous estimates based on projected changes in surface conditions (Hayhoe et al. 2004).

---

<sup>1</sup> NCAR CCSM3 is the National Center for Atmospheric Research Community Climate System Model, version 3.

We also hope to make these projections available to impact researchers in other fields, to estimate changes in other areas such as energy use or wildfire that may also be affected by atmospheric circulation patterns.

## 2.0 Background

Estimates of climate change impacts generally depend on projections of changes in local surface conditions such as temperature, precipitation, and humidity (Hayhoe et al. 2004). However, the intensity and duration of local surface weather conditions such as extreme temperature and humidity are often directly related to the frequency and persistence of oppressive air masses overhead (Sheridan and Kalkstein 2004). In turn, large-scale air masses tend to produce a consistent set of surface parameters that can result in specific impacts. In California, for example, a high-pressure system over the Great Basin, combined with a low-pressure system offshore, can result in the high temperatures, dry conditions, and strong inland winds that favor Santa Ana events (Miller and Schlegel 2006). Other circulation patterns can be linked to impacts such as heat waves, droughts, elevated heat-related mortality rates, and risk of extreme precipitation and flood events (e.g., Greene 1996; Huth et al. 2000; Meehl and Tebaldi 2004).

By design, atmosphere-ocean general circulation, or global climate, models (AOGCMs) are better suited to simulate the characteristics of large-scale air masses than local surface conditions. A major reason for this is their resolution, which limits both the topography and the scale of the physical processes that can be dynamically resolved by the model. The resolution of AOGCMs is typically on the order of several hundred kilometers, leading some to fear that “the rush to emphasize regional climate does not have a scientifically sound basis” (Henderson-Sellers 2008). AOGCM resolution is sometimes considered insufficient to distinguish between coastal versus inland conditions, particularly in a topographically diverse state such as California. The current AOGCM resolution, however, is more than adequate to identify the large-scale circulation patterns that cover up to one-half the North American continent at once (Figure 1). For this reason, we hypothesize the following: first, that large-scale atmospheric circulation patterns identified in reanalysis fields can be linked to surface conditions known to be related to specific weather-related impacts, characterized by “air mass” type; second, that climate models may be able to reproduce observed large-scale atmospheric circulation patterns better than they are able to simulate local- to regional-scale surface conditions; and third, that model simulations of changes in large-scale circulation patterns can serve as a reliable indicator of future impacts. Here, we evaluate the first of these two hypotheses in order to establish the basis for examination of the third in future work.

## 3.0 Data and Methods

As a first step towards evaluating these hypotheses, we clustered 500-mb and 700-mb geopotential and 850-mb temperature fields from ERA-40 reanalysis and CCSM AOGCM simulations for the period 1958–2002 into the dominant daily patterns using the principal components and clustering analysis described below. Each cluster identified from the reanalysis data represents a daily circulation or weather pattern that occurs frequently over North America.

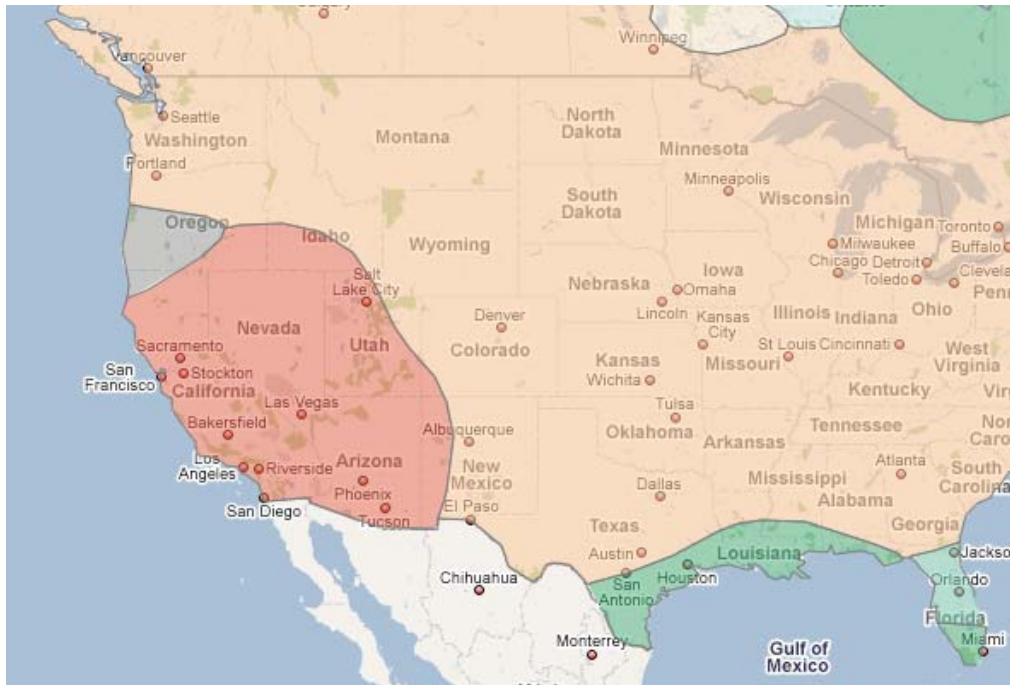


**Figure 1. This map of the air masses covering the western part of the United States on June 21, 2008, shows most of California covered in a hot, “Dry Tropical” air mass that can likely be associated with increased wildfire risk, heat stress, and demand for air conditioning**

We then associated these weather patterns with the surface occurrence of oppressive Spatial Synoptic Classification (SSC) air masses (described in Section 3.3) based on long-term weather station records for the same time period. We next assessed whether these patterns were associated with elevated heat-related mortality rates on the ground for seven California cities (San Francisco, San Diego, Alameda, Bakersfield, Fresno, Sacramento, and Los Angeles). Each of these data sources and methods is described further below.

### 3.1. Upper-Air Circulation Fields

The reanalysis fields used to identify dominant historical daily circulation patterns are the European Centre for Medium-Range Weather Forecasts (ECMWF)/ERA-40 data, available at daily resolution for the period 1958 to 2002 (Källberg et al. 2004). ERA-40 output fields were generated by the ECMWF IFS C423r4 model at a resolution of  $1.125^\circ \times 1.125^\circ$  and 60 levels in the vertical (Källberg et al. 2004). Recent evaluations confirm that the quality of the reanalysis product is generally high when compared to upper-air in situ observations (e.g., Simmons et al. 2004).

We also identify atmospheric circulation patterns as simulated by historical total-forcing runs from the NCAR CCSM3 (Collins et al. 2005). The CCSM3 is a fully coupled AOGCM with

atmosphere, ocean, sea ice, and land surface components, capable of producing stable climate simulations on the order of thousands of years. Grid resolution for the CCSM3 is T85 (approximately  $1.4^\circ \times 1.4^\circ$ ) over land and  $1^\circ$  over the ocean.

Our analysis is based on daily data for the 44-year time period for which ERA-40 fields are available, from 1958 through 2002. Historical CCSM simulations are based on the standard 20C3M scenario, which represents the best available estimates of twentieth-century total (anthropogenic + natural) forcing. As such, the 20C3M scenario includes observed historical emissions of carbon dioxide, methane, and other greenhouse gases; sulphate aerosols, soot, and other particulates; and other radiatively-active species produced by human activities such as nitrogen oxides and carbon monoxide. The historical scenario also includes observed changes in solar output and emissions from natural sources such as volcanoes, wetlands, and soils.

For this study, we focus on the region covering the North American continent. Both datasets were up-scaled to cover this region with a uniform  $5^\circ \times 5^\circ$  grid. Due to the size of North America and the spatial autocorrelation among adjacent grid points, this reduction in scale is unlikely to negatively affect results. Rather, it provides a first-order smoothing mechanism to facilitate identification of large-scale patterns from the day-to-day variability in geopotential height and temperature fields.

### **3.2. Principal Components and Cluster Analysis of Reanalysis and Climate Model Output**

Daily fields of geopotential heights ( $Z_g$ ) are frequently used to define atmospheric patterns (e.g., Vrac et al. 2007 and references therein). In this study, we cluster daily fields of  $Z_g$  at 500 mb and 700 mb and temperature ( $T$ ) fields at 850 mb to determine the atmospheric structures dominant in each. Circulation patterns can then be compared between pressure levels, and between reanalysis fields and simulated AOGCM output. In light of the extensive comparisons that can be made, in this study we focus on showing only the circulation patterns resulting from clustering of the 700 mb  $Z_g$  fields from ERA-40 reanalysis data and CCSM3 simulations. To assess the validity of CCSM3 simulations of historical data, the CCSM3 simulations were clustered independently from the ERA-40 data. The sole constraint was that the number of clusters identified in CCSM3 simulations be identical to those identified from ERA-40 fields.

The two-step procedure used here, consisting of principal components analysis (PCA) followed by cluster analysis (CA), is typical of studies that attempt to identify upper-air circulation patterns (Vrac et al. 2007). As the seasonal cycle of weather patterns is important to this study, geopotential-height values were not de-seasonalized prior to the PCA and CA steps.

Principal components analysis was performed on the 220 data points of ERA-40 and CCSM 700-mb geopotential height fields re-gridded to a uniform five-degree grid over the North American continent, as described above. The PCA yielded 19 principal components (PCs) for ERA-40 and 17 for CCSM with an eigenvalue of 1 or greater. Together, the PCs explained 95% of the day-to-day variance in geopotential height for ERA-40 and 96% for CCSM. The smaller number of PCs identified from CCSM fields and the slightly greater percentage of the variance these accounted for suggests a slight tendency for the CCSM simulations to underestimate day-to-day variance as compared to ERA-40.

The PCs identified for ERA-40 and CCSM were then each separately clustered using an agglomerative hierarchical clustering procedure within the statistical software program SPSS, yielding 12 clusters. The selection of 12 clusters was initially decided for the reanalysis data set based on Schwarz's Bayesian Information Criterion (BIC). For the CCSM data set, the same total number of clusters was chosen *a priori* to enable direct comparison of the two data sets. Similar to previous studies focusing on seasonal patterns (Vrac et al. 2007), this approach yielded four main types of patterns that could be categorized by their predominant monthly frequencies: winter, summer, and transition patterns to and from these two dominant seasons.

### 3.3. Spatial Synoptic Classification

The Spatial Synoptic Classification (SSC) system automatically classifies each day at a surface weather observing station into one of a number of air masses or weather types based on six-hour temperature, dew point, pressure, wind, and cloud cover, based on initial subjective air mass "seed day" identification<sup>2</sup> (Sheridan 2002). Here, SSC is utilized to identify the dates of "oppressive air masses," defined as air masses or weather types for which mean mortality rates in that location are statistically significantly above what would be the average condition. As shown in Table 1, the SSC identifies eight types of surface air mass conditions. Two of these air masses (DT and MT+) are associated with elevated mortality rates for many California urban areas (Table 3).

The SSC has been successfully utilized in many of the authors' operational heat watch-warning systems (e.g., Sheridan and Kalkstein 2004). These systems help protect urban populations from extreme heat events by identifying the air masses most significantly correlated with increasing mortality. When oppressive air masses are identified, heat alerts or warnings are declared, and mitigation plans are put into effect. Research has shown a statistically significant decrease in mortality rates in Philadelphia following the introduction of a heat-watch warning system in 1995 (Ebi et al. 2004). Thus, the systems are considered to be a quality adaptive response to excessive heat at present and into the future assuming a climate change (EPA 2006).

Observational evidence shows the health-weather relationship varies by time of year, with more people susceptible to early-season heat waves (Sheridan and Kalkstein 2004; Hajat et al. 2002). The vulnerability of urban populations to extreme heat also varies significantly by location, with inland cities more accustomed to heat extremes displaying a lower sensitivity than coastal cities with more typically moderate weather (Hayhoe et al. 2004). For those reasons, the air masses within the SSC are designed to change in character both spatially and temporally. For example, July mean 2 p.m. PDT temperature on "Dry Tropical" (DT) air mass days is 36°C (98°F) in Sacramento, whereas at San Francisco it is 30°C (86°F). In May, the respective city values are 31°C (88°F) and 28°C (82°F). The fact that surface weather conditions within air mass designations modify through the seasonal cycle is key to ensuring that the SSC can determine the impact of oppressive air masses on human health in a relative, rather than absolute, way.

---

<sup>2</sup> For more information on the SSC, see <http://sheridan.geog.kent.edu/ssc.html>.

**Table 1. Spatial synoptic classification (SSC) classes and typical characteristics and geneses in California**

<b>DP (dry polar)</b>	Synonymous with the traditional cP air mass classification. This air mass is uncommon in California, and is associated with clear, dry conditions.
<b>DM (dry moderate)</b>	Mild and dry. It has no traditional analog, but is often found with zonal flow in the middle latitudes. In California, it is very common in summer, associated with the typical stagnant, summer pattern along the coast.
<b>DT (dry tropical)</b>	Similar to the cT air mass, it represents the hottest and driest conditions found at any location. DT is very common in California's interior, and generally only appears along the coast in offshore wind events.
<b>MP (moist polar)</b>	A large subset of the mP air mass. It arises in California with strong northwesterly advection off of the Pacific.
<b>MM (moist moderate)</b>	Considerably warmer and more humid than MP. MM occurs in California with typical onshore wind conditions.
<b>MT (moist tropical)</b>	Analogous to the traditional mT air mass, is warm and very humid. It is typically found in California with strong southwesterly "Pineapple Express" flow off the Pacific.
<b>MT+ (moist tropical plus)</b>	A subset of MT where both morning and afternoon temperatures are above seed day means, and thus captures the most "oppressive" subset of MT days.
<b>TR (transitional)</b>	Days in which one air mass yields to another.

### 3.4. Mortality Data

Daily mortality data used to estimate the effects of oppressive air masses on California's urban population were obtained from the National Center for Health Statistics for the period 1975 to 2004 for the nine metropolitan areas shown in Table 2. These areas are defined to conform to the U.S. Census Bureau metropolitan area definition (U.S. Census 2008).

Heat-related mortality can be attributed to a broad range of secondary categories. This results in mortality within many categories increasing on oppressively hot days (e.g., Semenza et al. 1996). For this reason, total daily mortality from all causes is included to assess the effects of oppressive air masses on heat-related mortality in nine of California's metropolitan areas.

**Table 2. Population (year 2000) by age group for the California metropolitan areas studied in this research**

	<65	65–74	75+
Fresno	829,711	48,842	43,963
Los Angeles	8,592,665	492,833	433,840
Oakland	2,137,694	130,421	124,442
Orange	2,565,526	148,702	132,061
Riverside	2,912,398	184,398	158,025
Sacramento	1,440,428	99,357	88,412
San Diego	2,500,083	160,059	153,691
San Francisco	1,503,555	115,488	112,140
San Jose	1,522,058	87,193	73,334

Deaths were stratified into three age groups: those under 65, those 65–74, and those 75 and older. To account for demographic and population changes over time, raw mortality values were standardized by converting daily mortality totals into rates per 100,000, relative to the population of each urban center. Linear interpolations between 10-year census values were used to estimate changes in annual population, from which mortality rates were calculated.

To account for the seasonal cycle in mortality, these mortality rates were then converted to proportions relative to the mean daily mortality rate by month. For example, for each day in June throughout the period of record, the total mortality rate for the day for those under 65 was compared to the mean June mortality rate of those under 65 across all June days to calculate a anomalous mortality percentage. Air masses for which anomalous mortality is statistically significantly above 0 (using a two-sample difference of means test) are deemed “oppressive.”

## 4.0 Results

### 4.1. Comparison of Reanalysis-based vs. AOGCM-based Circulation Patterns

ERA-40 daily 500-mb and 700-mb geopotential height fields and 850-mb temperatures were each clustered into 12 patterns, with the number of patterns being determined by the Bayesian Information Criterion. Each pattern represents a typical weather system that recurs frequently over North America either during winter, summer, or during the transitional period to and from these two dominant seasons (Figure 2).

Each day of the year was then assigned to one of these patterns, and the average monthly frequencies of each pattern was calculated. Geopotential height and temperature fields for the days assigned to each pattern could then be averaged over the entire time period (1958–2002) to produce a spatial map of what each cluster or circulation pattern actually looks like (Figure 3). For simplicity, only the results of the 700-mb clustering are shown here, as similar conclusions can be drawn from analysis of higher- and lower-level clusters.

For the CCSM3 output fields, the same total number of clusters was chosen *a priori* to enable direct comparison of the two data sets. After the initial clustering, however, one winter transitional CCSM3 pattern (no. 11) had to be split into two patterns in order to match

observed frequencies for ERA-40 patterns 4 and 7, while two CCSM3 summer patterns (no. 1 and 2) had to be merged to match observed frequencies for ERA-40 pattern 2. The order of the CCSM3 patterns as compared to ERA-40 was primarily an artifact of the clustering procedure; hence, the order of the patterns was rearranged by matching monthly frequencies and spatial patterns to ERA-40 clusters to produce a one-to-one match between observed and model-simulated patterns (Table 3).

By matching each CCSM3 pattern with its corresponding ERA-40 pattern, monthly frequencies of CCSM3 patterns could then be directly compared with ERA-40 pattern frequencies. In Figure 2, monthly frequencies for matching CCSM3 and ERA-40 patterns for winter, winter transitional, summer, and summer transitional are plotted. This figure shows how each seasonal pattern exhibits a distinctive temporal signature, which is generally reproduced by the AOGCM-based patterns. We therefore conclude that CCSM3 simulations are able to successfully reproduce the month-to-month frequency of circulation patterns evident from reanalysis fields.

Nonetheless, there are some clear biases in the AOGCM pattern frequencies relative to ERA-40. These can be seen partially in the individual patterns, but more clearly when the patterns for the four seasons are aggregated (Figure 2, last row). For example, the high frequency of winter patterns in December and January are not as pronounced in CCSM3 simulations as in ERA-40. In CCSM3 simulations, the frequency of winter and summer transitional patterns also peaks too early in the year, suggesting spring conditions emerge sooner in the model than in reality; although their frequencies during the autumn months are quite realistic. Similarly, the CCSM3-based summer patterns also show higher frequencies than observed during the months of May and June, confirming the initial results from Vrac et al. (2007) that the CCSM3 summer pattern tends to emerge too early in the year.

Identifying physical biases in the frequency and timing of seasonal circulation patterns as opposed to merely quantifying statistical biases in surface conditions, provides valuable insight into the physical shortcomings of global models such as CCSM3. Although these biases certainly affect model simulations of surface conditions, they may not be evident from directly comparing observed and modeled surface characteristics. If these biases can be accounted for when examining projected future changes in the frequency and duration of these patterns, it could be possible to significantly improve the predictive capacity of global models. If unaccounted for, however, biases such as these could lead to an over-estimate of the projected trend towards earlier emergence of summer patterns, for example.

**Table 3. ERA-40 patterns and CCSM3-based matches**

ERA-40 pattern	Description	CCSM match
1	Summer	3
2	Summer	2
3	Transition from/to spring/fall	4
4	Transition from winter	11
5	Transition to/from summer	5
6	Winter	12
7	Transition from winter	11
8	Winter	8
9	Winter	7
10	Winter	10
11	Transition to/from winter	6
12	Transition to winter	9

In Figure 3, we compare the spatial characteristics of the clusters. Again, we conclude that in most cases CCSM3-simulated clusters are recognizable facsimiles of the clusters identified in reanalysis fields. In general, summer and summer transitional patterns appear to match well. Winter patterns, however, exhibit strong troughs that are offset in CCSM3 simulations as compared to ERA-40. In contrast, CCSM3-based winter transitional patterns tend to exhibit very zonal flow compared to the more defined patterns seen in reanalysis fields.

Not all differences between ERA-40 and CCSM3 clusters should be attributed to AOGCM deficiencies. Previous studies (Vrac et al. 2007) have shown that clusters generated from two distinct sets of reanalysis fields (e.g., ERA-40 versus National Centers for Environmental Prediction [NCEP]) or even from reanalysis fields from the same source, but using two different spatial scales can result in patterns that differ notably from each other. To quantify the extent to which ERA-40/CCSM3 differences are truly due to model biases, in future work we intend to compare spatial and temporal patterns of NCEP-based clusters with ERA-40 and CCSM3 with other AOGCMs.

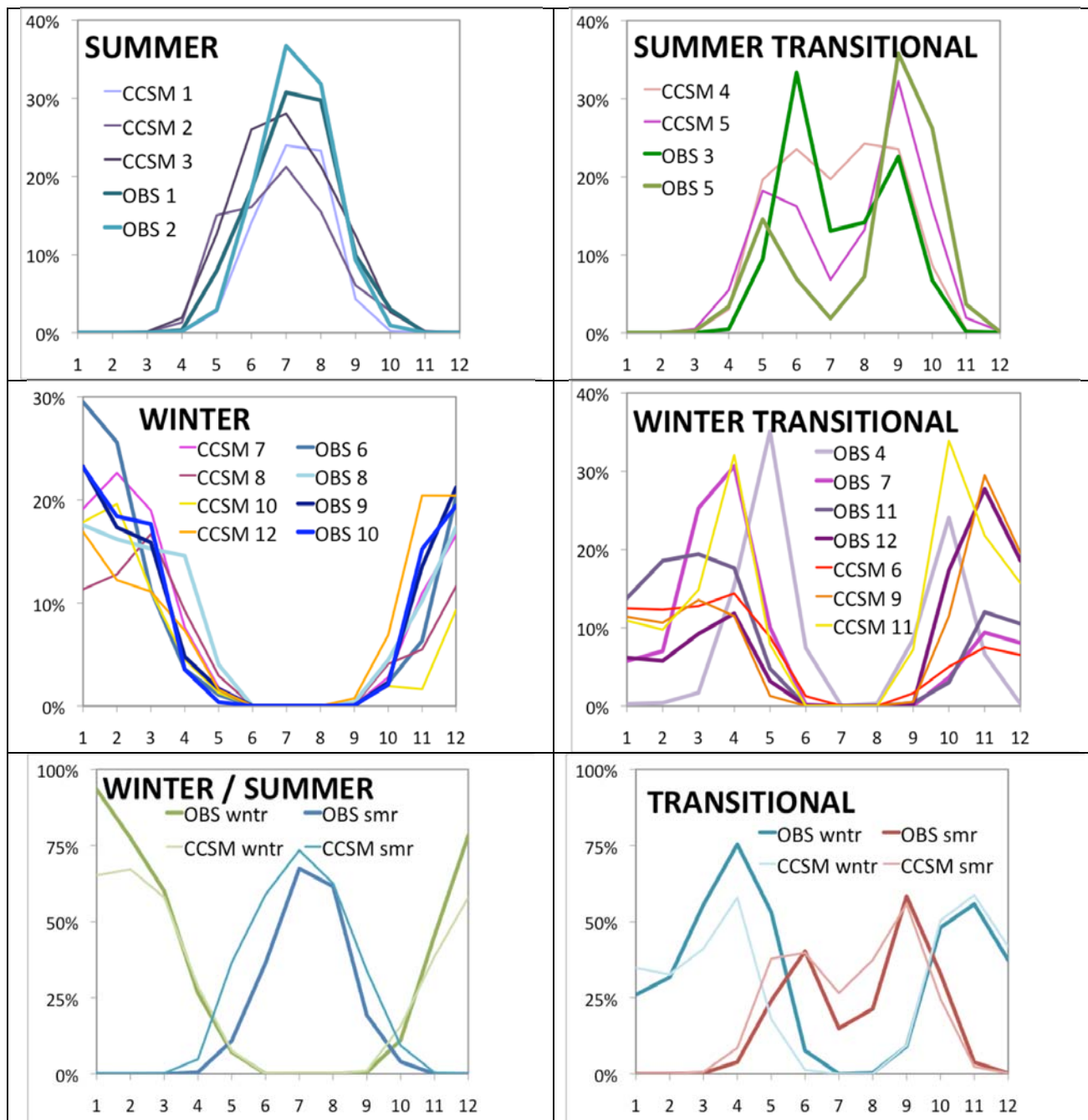
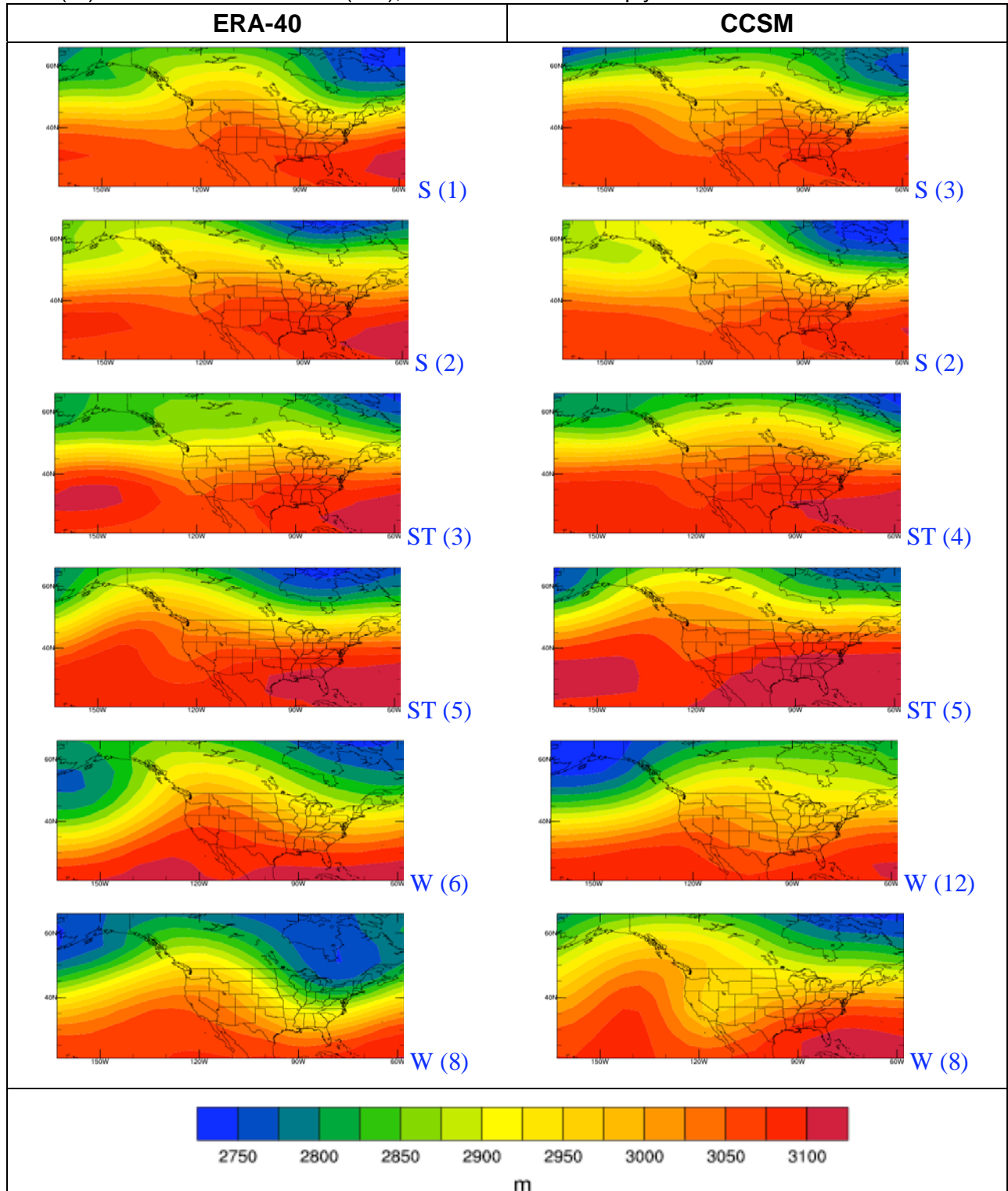
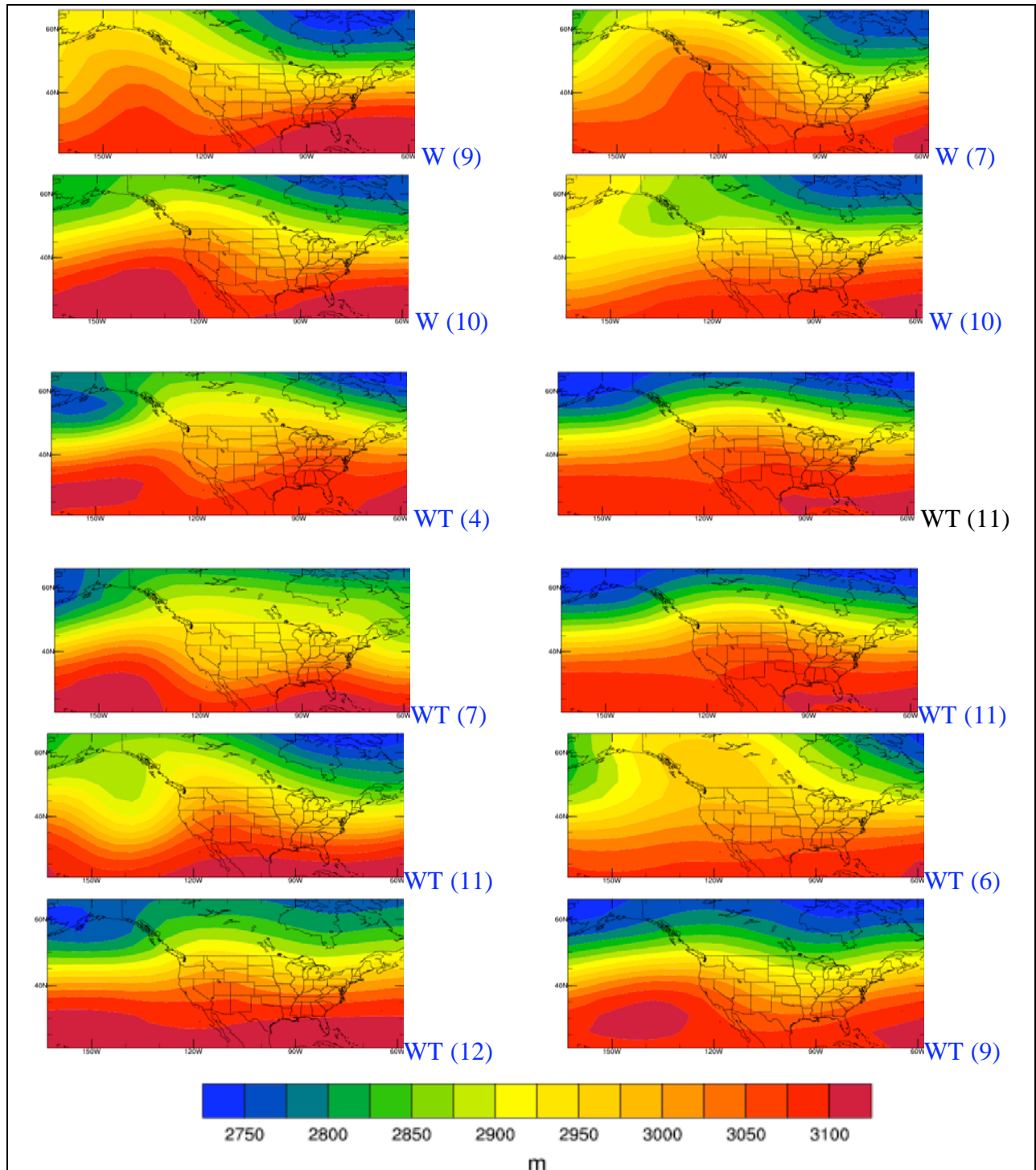


Figure 2. Monthly frequency of ERA-40 and CCSM-based daily circulation patterns for 1958–2002. The proportion of days in each month belonging to each pattern is shown on the y-axis, while months are shown on the x-axis, from January (1) to December (12).

(W) and Winter Transitional (WT), while the number simply indicates the cluster number.





**Figure 3. Spatial patterns for matching ERA-40 and CCSM clusters based on 700 mb geopotential heights. Patterns are grouped by Summer (S), Summer Transitional (ST), Winter (W), and Winter Transitional (WT), while the number simply indicates the cluster number.**

## 4.2. Mortality Variability by Air Mass Across California

Similar to previous research, for most cities in California we find that consistent statistically significant increases in mortality do occur with two air masses, Moist Tropical Plus (MT+) and Dry Tropical (DT) (Table 3). For Riverside and Fresno the increase is not statistically significant, although mortality ratios do increase for these two air mass types.

**Table 3. Mean anomalous mortality (expressed as a percentage relative to the seasonal average) on Dry Tropical and Moist Tropical Plus days for the period of April–October for nine urban centers in California, separated by age (under 65, between 65 and 74, and over 74 years of age). Also shown are the average frequencies for which each air mass type (Dry Tropical and Moist Tropical Plus) occurs over each city during this period. A frequency of 10%, for example, means that 10% of the days from April to October fall into that air mass category.**

	Dry Tropical				Moist Tropical Plus			
	<65	65–74	>74	Freq.	<65	65–74	>74	Freq.
Los Angeles	+9.6%*	+9.4%*	+10.8%*	1.9%	+5.9%*	+6.8%*	+10.2%*	1.0%
Orange	+9.7%*	+8.5%*	+2.8%	1.9%	+9.1%*	+12.6%*	+6.4%*	1.0%
Sacramento	+4.4%*	+2.3%	+3.5%*	19.9%	+5.8%*	+10.0%*	+5.7%*	0.2%
San Francisco	+4.4%*	+5.4%*	+8.2%*	4.2%	-9.2%	-10.2%	+15.7%*	0.2%
Fresno	+2.4%	+0.3%	+1.5%	37.3%	-2.0%	-9.9%	-3.2%	0.3%
San Diego	+22.1%*	+6.0%*	+2.6%	1.7%	+12.0%*	+10.4%*	+10.4%*	1.3%
Oakland	-2.6%	-8.3%*	-1.3%	4.2%	-5.6%	+10.4%	+16.6%*	0.2%
Riverside	-4.2%	-0.7%	+0.8%	37.3%	+4.3%	0.0%	-0.8%	0.3%
San Jose	+4.2%*	+6.1%*	+9.0%*	4.2%	+1.0%	+16.8%*	+13.0%*	0.2%

\* indicates values that mortality increases are statistically significant at a = .05.

Significant spatial and age-related variability in vulnerability is apparent from one city to the next. As supported by much previous research (e.g., Conti et al. 2005), increases in mortality are generally larger across the older age groups, particularly for MT+, and in cities with more moderate climates. The most consistently vulnerable city is Los Angeles, where the DT air mass is associated with approximately a 10% increase in mortality across all age groups; with MT+ the increased mortality ranges from 6% to 10%. Around the Bay Area, San Francisco and San Jose show larger increases in mortality than Oakland. Inland, although the absolute numbers are lower (2% to 4%), Sacramento shows statistically significant increases in mortality on DT days, an observation made more significant by its much larger frequency of occurrence compared with coastal locations. Across other inland locations, however, the heat-mortality relationship appears weaker.

## 4.3. Historical Frequency of Oppressive Air Mass Occurrence by Reanalysis Cluster

Last, we quantified the relationship between oppressive SSC air mass occurrence (DT or MT+) on the ground and reanalysis cluster frequencies at 700 mb to identify the clusters most frequently associated with historical oppressive air mass events. In Figure 4, the proportion of days during the California warm season (April through October) that were classified as “oppressive” for the period 1958–2002 are plotted for each cluster type. Results are shown

individually for coastal (a) and inland (b) cities as the correlation of oppressive air mass events with cluster types differ significantly.

Three important results emerge from Figure 4. First, the historical record shows a significantly larger proportion of oppressive air mass events for inland cities such as Sacramento, Fresno, and Bakersfield, as compared to coastal cities such as San Francisco, Oakland, Los Angeles, and San Diego.

Second, for all cities certain clusters are clearly associated with high percentages of oppressive days, and others with low.

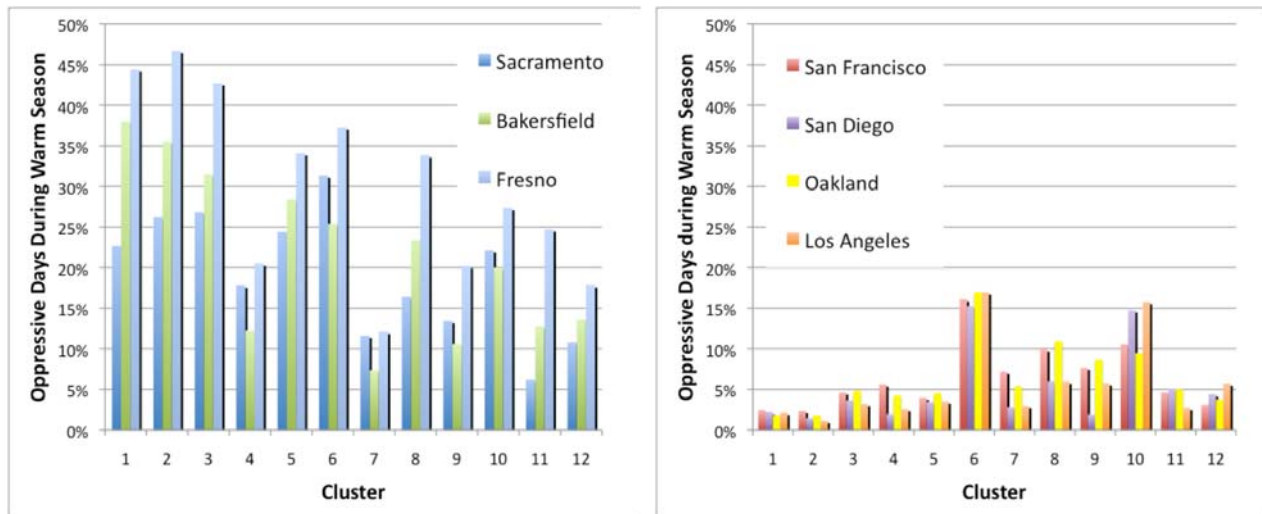


**Figure 4. Observed frequency of oppressive air mass days during the months of April to October by ERA-40 cluster for (a) inland cities, and (b) coastal cities**

Third, and perhaps most interestingly, the clusters most frequently associated with oppressive air mass events for inland cities are not the same clusters associated with these types of events for coastal cities, and they have very different seasonal signatures. Specifically, clusters 1, 2, and 3 (and, to a lesser extent, 5 and 6) have the highest frequency of oppressive days for inland cities. These clusters are all typical of summer weather. For Fresno, over 40% of days rank as offensive or oppressive for clusters 1 through 3. In contrast, the highest frequency of oppressive days for coastal cities are associated with clusters 6 and 10. Table 1 reveals that these clusters are typical of winter conditions. As shown in Figure 2, clusters 6 and 10 are relatively rare during summer months. If these are the clusters that bring oppressive conditions to coastal cities, this suggests that part of the reason for the low frequency of these events is because these clusters are more typical during cooler winter than warmer summer conditions.

Further information, especially for transitional spring and autumn seasons, can be derived by separating out the proportion of oppressive days per cluster by month (Table 4). This provides

a more nuanced perspective on the relationship between cluster type and oppressive air mass conditions.

For example, Cluster 1, with a broad mid-level ridge over the entire southwestern United States (Figure 3), is relatively common in summer where the likelihood of an oppressive air mass is similar to the overall likelihood of Cluster 1. Incidence of Cluster 1 during spring, which is much less common, is associated with a significant increase in the likelihood of an oppressive air mass at the surface for both coastal and inland cities. At San Francisco and Oakland, 24% of Cluster 1 days in April are oppressive (versus 7% and 6% across all clusters); in Bakersfield, 56% of days are oppressive (versus 10% overall). Lesser, but still statistically significant, increases in likelihood occur in May as well.

Into the autumn, different clusters are associated with increased likelihood of an oppressive air mass. Clusters 6 and 10 are associated with around a doubling (inland) to tripling (coastal) of oppressive air mass conditions in October, and to a lesser extent, September. Clusters 6 and 10 are similar to Cluster 1 in terms of the broad ridge, although in this case it is centered over (6) or west of (10) California and Nevada. Interestingly, in autumn, Cluster 1 is still common, but only associated with slight increases in likelihood of an oppressive air mass.

Across both transitional seasons, Cluster 8, featuring a ridge axis off the Pacific Coast, is associated with an increased likelihood of oppressive air masses in coastal regions more than in the interior. This is particularly true in autumn, when the oppressive air mass likelihood nearly triples in San Francisco in October (an 18% chance of an oppressive air mass in autumn in Cluster 8 versus 7% overall) but remains unchanged in Sacramento (24% chance in autumn in Cluster 8 versus 24% chance overall).

Cluster 3, which reaches peak frequency in early summer, and Cluster 5, which reaches peak frequency in September and October, both have a broad western ridge in their mean patterns, with an advancing trough approaching the Pacific Coast. These clusters are affiliated with the opposite relationship to oppressive air mass events as Cluster 8. Inland, large increases in oppressive air mass likelihood are seen (e.g., Cluster 8, Sacramento, 33% versus 24% and Fresno, 38% versus 27%, in October), with no increase in likelihood seen in coastal locations.

During the peak summer months of July and August, very little relationship is seen between 700-mb cluster and oppressive air mass likelihood. Instead, stronger correlations are seen between 850-mb temperature clusters and oppressive air mass likelihood, with the highest likelihood associated with broad thermal ridges in the lower troposphere (not shown).

## 5.0 Discussion and Conclusions

Of the twelve circulation patterns identified in ERA-40 reanalysis fields for 700 mb geopotential height fields, we have identified three upper-air patterns (clusters) that are associated with high frequencies of oppressive air mass events at the surface for coastal cities, and two for inland cities. As shown in Table 4, upper-air patterns 6 and 10 are highly associated with an increased likelihood of surface-level oppressive air mass events for the coastal cities of San Diego, Los Angeles, Oakland, and San Francisco, though the overall likelihood is still lower than for inland cities. In contrast, upper-air patterns 1, 2, and 3 are most highly associated with surface-level oppressive air mass events for the inland cities of

Sacramento, Fresno and Bakersfield, with up to 44% of the days being classified as oppressive for pattern 1 and 47% for pattern 2.

Interestingly, the patterns associated with coastal events are typical of winter months, whereas the patterns associated with inland events are typical of summer conditions. This observation suggests a possible distinction in future impacts between coastal and inland California cities, as winter versus summer circulation patterns may be affected very differently under future climate regimes.

Although the resemblance is not perfect, CCSM3 is clearly able to simulate the approximate spatial patterns and monthly frequencies of the dominant twelve annual circulation patterns over North America. Thus, at least one climate model appears capable of reproducing the historical characteristics of upper-air circulation patterns associated with surface oppressive air masses and extreme heat-related impacts over California. We are currently assessing the ability of other AOGCMs for which daily geopotential height and temperature fields are available to reproduce observed circulation patterns. We are also quantifying the extent to which the differences between the ERA-40 reanalysis patterns and the CCSM3 patterns may be due to deficiencies in the ability of global climate models to represent reality, as opposed to error in the reanalysis fields, which themselves are an imperfect representation of reality.

As noted, analyses for 500-mb Zg and 850-mb T fields resulted in similar findings to the 700-mb analysis presented here. When likelihood of an oppressive air mass event is associated with specific combinations of clusters at the three levels (e.g., days that are classified into the most “oppressive” for 500-mb, 700-mb, and 850-mb clusters), the frequency of oppressive air masses increases significantly, although sample size becomes a key detriment in certain cases. Nevertheless, it is clear that mid-tropospheric flow categorization combined with lower-tropospheric thermal classification can be successfully used to forecast the likelihood of oppressive air mass conditions. Hence, future work will combine the three pressure levels into one predictive framework.

Our ultimate goal is to construct a series of future projections of changes in air mass frequencies based on simulations of daily geopotential height and temperature fields for higher and lower emission scenarios. The method described here will first be validated by dividing the historical period into a training and a prediction period to test the predictive capacity of the observed correlations between surface-level oppressive air masses and upper air fields. Assuming adequate predictive capacity, the AOGCM projections of simulated future 500-mb Zg, 700-mb Zg, and 850-T fields will then be categorized into clusters using discriminant function analysis based on the cluster definitions from the historical model runs. These clusters will be used to develop estimates of the likely changes in the risk of oppressive air mass days at the surface, enabling an assessment of the impacts of changing risk on heat-related mortality and related impacts for California’s urban centers.

**Table 4. Proportion of oppressive air mass occurrence, by city and 700-mb cluster, for the ERA-40 reanalysis period of record from 1958–2002 for the warm season (April–October)**

City	Cluster											
	1	2	3	4	5	6	7	8	9	10	11	12
April												

Sacramento	24%	0%	5%	12%	8%	20%	11%	17%	8%	9%	3%	4%
San Francisco	24%	0%	5%	6%	5%	10%	8%	12%	8%	5%	5%	4%
Bakersfield	56%	20%	10%	5%	20%	12%	5%	18%	11%	13%	11%	8%
San Diego	12%	0%	10%	2%	0%	18%	2%	10%	4%	9%	4%	4%
Oakland	24%	0%	5%	4%	5%	16%	5%	14%	8%	7%	4%	5%
Los Angeles	12%	0%	5%	3%	2%	16%	3%	9%	8%	13%	2%	8%
Fresno	64%	40%	35%	16%	20%	24%	11%	30%	15%	15%	21%	13%
n	25	5	20	245	61	50	413	105	53	55	160	158
<b>May</b>												
Sacramento	21%	15%	28%	17%	14%	31%	9%	8%	11%	0%	11%	10%
San Francisco	7%	3%	7%	6%	1%	6%	5%	2%	16%	0%	5%	0%
Bakersfield	39%	23%	28%	16%	24%	25%	9%	25%	16%	20%	11%	10%
San Diego	2%	2%	2%	1%	1%	0%	1%	0%	0%	0%	2%	2%
Oakland	3%	0%	4%	4%	0%	6%	4%	2%	5%	0%	8%	0%
Los Angeles	1%	0%	4%	1%	0%	0%	1%	2%	0%	0%	0%	2%
Fresno	46%	48%	45%	25%	30%	69%	11%	29%	37%	20%	35%	14%
n	177	60	121	540	169	16	129	48	19	5	62	49
<b>June</b>												
Sacramento	23%	23%	28%	16%	12%	0%	0%	9%				50%
San Francisco	3%	3%	7%	4%	3%	0%	0%	0%				0%
Bakersfield	36%	36%	31%	11%	22%	0%	17%	27%				0%
San Diego	1%	0%	2%	0%	1%	0%	0%	0%				0%
Oakland	2%	2%	5%	1%	2%	0%	0%	0%				0%
Los Angeles	1%	1%	2%	0%	1%	0%	0%	0%				0%
Fresno	48%	49%	46%	20%	20%	0%	0%	36%				50%
n	295	303	364	226	142	1	6	11				2
<b>July</b>												
Sacramento	22%	26%	22%	0%	10%							
San Francisco	1%	2%	3%	0%	0%							
Bakersfield	43%	39%	36%	0%	32%							
San Diego	1%	1%	2%	0%	0%							
Oakland	1%	2%	3%	0%	0%							
Los Angeles	1%	1%	0%	0%	0%							
Fresno	47%	51%	50%	67%	32%							
n	549	567	235	3	41							

**Table 4. (continued)**

	August					September								October															
Sacramento	22%	29%	21%	55%	17%	26%	30%	35%	31%	30%	33%	0%	50%	50%	67%	0%	0%	29%	25%	27%	17%	33%	44%	22%	24%	23%	44%	11%	15%
San Francisco	0%	1%	0%	0%	1%	3%	3%	5%	8%	5%	0%	0%	0%	50%	33%	0%	0%	5%	13%	5%	5%	7%	29%	7%	18%	0%	19%	3%	3%
Bakersfield	36%	35%	34%	27%	32%	31%	33%	34%	18%	29%	50%	0%	100%	0%	33%	0%	0%	30%	16%	20%	9%	32%	38%	19%	27%	7%	31%	23%	18%
San Diego	1%	2%	3%	0%	0%	8%	3%	8%	5%	5%	17%	0%	0%	0%	33%	0%	0%	8%	16%	4%	4%	6%	18%	10%	6%	0%	25%	14%	5%
Oakland	0%	1%	1%	0%	1%	3%	3%	9%	10%	6%	0%	0%	0%	50%	33%	0%	0%	7%	13%	6%	6%	8%	24%	12%	18%	10%	13%	6%	4%
Los Angeles	1%	1%	2%	0%	0%	9%	2%	7%	3%	4%	0%	0%	0%	0%	33%	0%	0%	6%	6%	5%	6%	7%	27%	8%	6%	7%	22%	11%	5%
Fresno	41%	45%	40%	18%	27%	38%	38%	41%	26%	40%	83%	25%	100%	50%	67%	0%	0%	41%	31%	24%	13%	38%	36%	20%	45%	17%	47%	23%	22%
n	559	465	205	11	155	185	159	288	136	555	6	4	4	2	3	2	6	97	32	109	328	356	45	59	33	30	32	35	239

## 6.0 References

- Collins, W., C. Bitz, M. Blackmon, G. Bonan, C. Bretherton, J. Carton, P. Chang, S. Doney, J. Hack, T. Henderson, J. Kiehl, W. Large, D. McKenna, B. Santer, and R. Smith. 2006. "The Community Climate System Model CCSM3." *Journal of Climate* 19: 2122–2143.
- Conti, S., P. Meli, G. Minelli, R. Solimini, V. Toccaceli, M. Vichi, C. Beltrano and L. Perini. 2005. "Epidemiologic study of mortality during the Summer 2003 heat wave in Italy." *Environmental Research* 98(3): 390–399.
- Ebi, K. L., T. J. Teisberg, L. S. Kalkstein, L. Robinson, and R. F. Weiher. 2004. "Heat watch/warning systems save lives: Estimated costs and benefits for Philadelphia 1995–1998." *Bulletin of the American Meteorological Society* 85:1067–1074.
- EPA. 2006. *Excessive Heat Events Guidebook*. Washington, D.C.: EPA 430-B-06-005, 52pp.
- Greene, J. S. 1996. "A synoptic climatological analysis of summertime precipitation intensity in the eastern United States." *Physical Geography* 17:401–418.

- Hajat, S., R. S. Kovats, R. W. Atkinson, and A. Haines. 2002. "Impact of hot temperatures on death in London: A time series approach." *Journal of Epidemiology and Community Health* 56:367–372.
- Hayhoe, K., D. Cayan, C. B. Field, P. C. Frumhoff, E. P. Maurer, N. L. Miller, S. C. Moser, S. H. Schneider, K. Nicholas Cahill, E. E. Cleland, L. Dale, R. Drapek, R. M. Hanemann, L. S. Kalkstein, J. Lenihan, C. K. Lunch, R. P. Neilson, S. C. Sheridan, and J. H. Verville. 2004. "Emissions pathways, climate change, and impacts on California." *Proceedings of the National Academy of Sciences* 101:12422–12427.
- Henderson-Sellers, A. 2008. The IPCC report: What the lead authors really think. *Talking Point, Environmental Research Web*. Available online at: <http://environmentalresearchweb.org/cws/article/opinion/35820>.
- Huth, R., J. Kysely, and L. Pokorna. 2000. "A GCM simulation of heat waves, dry spells, and their relationships to circulation." *Climatic Change* 46:29–60.
- Källberg, P., A. Simmons, S. Uppala, and M. Fuentes. 2004. The ERA-40 archive. A ECMWF report, available online at: [www.ecmwf.int/publications/library/ecpublications/pdf/era40/ERA40\\_PRS17.pdf](http://www.ecmwf.int/publications/library/ecpublications/pdf/era40/ERA40_PRS17.pdf).
- Meehl, G., and C. Tebaldi. 2004. "More intense, more frequent, and longer lasting heat waves in the 21st century." *Science* 305:994–997.
- Miller, N., and N. Schlegel. 2006. "Climate change projected fire weather sensitivity: California Santa Ana wind occurrence." *Geophysical Research Letters* 33: L15711.
- Semenza, J. C., C. H. Rubin, K. H. Falter, J. D. Selanikio, W. D. Flanders, H. L. Howe, and J. L. Welhlem. 1996. "Heat Related Deaths during the July 1995 Heat wave in Chicago." *New England Journal of Medicine* 335:84–90.
- Sheridan, S. C. 2002. "The Redevelopment of a Weather-Type Classification Scheme for North America." *International Journal of Climatology* 22:51–68.
- Sheridan, S. C., and L. Kalkstein. 2004. "Progress in Heat Watch-Warning System Technology." *Bulletin of the American Meteorological Society* 85:1931–1941.
- Simmons, A. J., P. D. Jones, V. D. Bechtold, A. C. M. Beljaars, P. W. Kallberg, S. Saarinen, S. M. Uppala, P. Viterbo, and N. Wedi. 2004. "Comparison of trends and low-frequency variability in CRU, ERA-40, and NCEP/NCAR analyses of surface air temperature." *Journal of Geophysical Research* 109: D24115.
- U.S. Census Bureau. 2008. U.S. Interim Projections by Age, Sex, Race, and Hispanic Origin. Available online at: [www.census.gov/ipc/www/usinterimproj/](http://www.census.gov/ipc/www/usinterimproj/). Accessed 24 August 2008.
- Vrac, M., K. Hayhoe, and M. Stein. 2007. "Identification and intermodal comparison of seasonal circulation patterns over North America." *International Journal of Climatology* 27:603–620.

## 7.0 Glossary

20C3M	a climate scenario
AOGCM	atmosphere-ocean general circulation, or global climate, model
BIC	Bayesian Information Criterion
CA	cluster analysis
CCSM3	Community Climate System Model, version 3
ECMWF	European Center for Medium Range Weather Forecasting
ERA-40	A project of the ECMWF
IFS	Integrated Forecasting System
mb	millibar
NCAR	National Center for Atmospheric Research
NCEP	National Centers for Environmental Prediction
PC	principal component
PCA	principal component analysis
PDT	Pacific Daylight Time
SPSS	statistical software program
SSC	Spatial Synoptic Classification
T	temperature
Zg	geopotential heights